Characterizing wet and dry fluids in temperature-entropy diagrams

J. A. White[a,b,*], S. Velasco[a,b]

[a] *Departamento de Física Aplicada, Universidad de Salamanca, 37008 Salamanca, Spain*
[b] *IUFFyM, Universidad de Salamanca, 37008 Salamanca, Spain*

Abstract

In this work we show that the shape of the liquid-vapor saturation curve in a $T_\mathrm{r} - s^*$ diagram ($T_\mathrm{r} = T/T_\mathrm{c}$ and $s^* = s/R$, with T_c the critical temperature, s the molar entropy and R the gas constant) for a given fluid is mainly governed by the acentric factor, ω, and the critical molar volume, v_c, of the fluid. The study uses as reference the point M where the saturated vapor curve in the $T_\mathrm{r} - s^*$ diagram changes its concavity, i.e. $(\mathrm{d}^2 s^{*\mathrm{g}}/\mathrm{d}T_\mathrm{r}^2)_\mathrm{M} = 0$. By analyzing the data provided by the National Standards and Technology (NIST) program RefProp 9.1 for 121 fluids, we find that, at this point, $T_\mathrm{Mr} \approx 0.81$ and the slope $\xi^*_\mathrm{M} = (\mathrm{d}s^{*\mathrm{g}}/\mathrm{d}T_\mathrm{r})_\mathrm{M}$ is well correlated with v_c, existing a threshold value $v_{\mathrm{c},0} \approx 0.22$ m^3 kmol^{-1} so that $\xi^*_\mathrm{M} < 0$ (wet fluid) for $v_\mathrm{c} < v_{\mathrm{c},0}$ and $\xi^*_\mathrm{M} > 0$ (dry fluid) for $v_\mathrm{c} > v_{\mathrm{c},0}$. This direct relation between v_c and the wet or dry character of a fluid is the main result of the present work. Furthermore, the dimensionless vaporization entropy at the reference point M, $\Delta_\mathrm{v} s^*_\mathrm{M} = s^{*\mathrm{g}}_\mathrm{M} - s^{*\mathrm{l}}_\mathrm{M}$, increases in a nearly linear way with ω.

Keywords: Temperature-entropy saturation curve, Saturation properties, Wet and dry fluids, Saturation heat capacities, ORC working fluids

*Corresponding author. Address: Departamento de Física Aplicada, Universidad de Salamanca, 37008 Salamanca, Spain. Tel: +34 923294436; fax: +34 923294584.
Email address: white@usal.es (J. A. White)

Nomenclature

$\Delta_{\mathrm{v}}h$	Molar enthalpy of vaporization, J/mol
ν	Molar volume, m^3/kmol
σ_{c}	Intermolecular separation at zero potential energy, nm
c_P	Isobaric molar heat capacity, J/(mol K)
c_{sat}	Molar heat capacity along the saturation line, J/(mol K)
N_A	Intermolecular separation at zero potential energy, nm
p	Pressure, MPa
R	Gas constant, 8.314472 J/(mol·K)
s	Molar entropy, J/(mol·K)
T	Temperature, K
Greek letters	
ω	acentric factor
ξ	Inverse of the slope of the saturated vapor curve, $\mathrm{J/(mol{\cdot}K^2)}$
Superscripts	
*	Dimensionless
g	Saturated vapor
l	Saturated liquid
Subscripts	
0	Reference value that separates wet fluids from dry fluids
1,2	Points for which $\xi^* = 0$
b	Normal boiling
c	Critical
M	Point for which $\xi^*(T_{\mathrm{r}})$ presents a maximum
r	Reduced
tp	Triple point
v	Vaporization
Acronyms	
CSP	Corresponding states principle
NIST	National Institute of Standards and Technology
ORC	Organic Rankine cycle

1. Introduction

Thermodynamic liquid-vapor saturation properties of working fluids affect efficiency, utility costs, maintenance and environmental impact of engineering systems such as vapor-compression based refrigeration, heat pump devices and Rankine cycles. In particular, the choice of working fluids is very important in organic Rankine cycles (ORC) [1]. An ORC works like a conventional Rankine cycle but uses an organic working fluid instead of water and it has been designed for producing electrical power from renewable energies (wind, solar, geothermal, biomass) or from low-temperature waste heat.

A crucial aspect for the selection of a working fluid in an ORC is its saturation liquid-vapor curve in a temperature-molar entropy ($T-s$) diagram. Depending on the slope, $\mathrm{d}T/\mathrm{d}s^{\mathrm{g}}$, of the saturated vapor branch, three types of fluids are considered: dry fluids with positive slopes, wet fluids with negative slopes, and isentropic fluids with nearly infinite slopes. Dry and isentropic organic fluids are usually used in ORC's because they do not present condensation after isentropic expansion in the turbine.

In 2004, Liu *et al.* [2] proposed to consider the inverse of the slope of the saturated vapor curve, $\xi = \mathrm{d}s^{\mathrm{g}}/\mathrm{d}T$, on the $T-s$ diagram in order to classify the fluids. After some simplifications, these authors derived for ξ the following temperature dependent expression

$$\xi = \frac{c_P^{\mathrm{g}}}{T} - \frac{1-(1-n)T_{\mathrm{r}}}{1-T_{\mathrm{r}}}\,\frac{\Delta_{\mathrm{v}}h}{T^2}\,, \tag{1}$$

where c_P^{g} is the isobaric molar heat capacity of the saturated vapor, $T_{\mathrm{r}} = T/T_{\mathrm{c}}$ the reduced temperature, being T_{c} the critical temperature, $\Delta_{\mathrm{v}}h$ is the molar enthalpy of vaporization, and $n \approx 0.38$ is the exponent appearing in the well-known Watson relation for the temperature dependence of $\Delta_{\mathrm{v}}h$ [3, 4]. Finally, Liu *et al.* [2] computed the value of ξ at the normal boiling temperature, T_{b}, of the fluid in order to predict its behavior in the turbine expansion process: $\xi_{\mathrm{b}} \equiv \xi(T_{\mathrm{b}}) < 0$, wet fluid; $\xi_{\mathrm{b}} \sim 0$, isentropic fluid; and $\xi_{\mathrm{b}} > 0$, dry fluid. In 2007, Invernizzi *et al.* [5] introduced a *parameter of molecular complexity* which

is equal to ξ expressed in reduced units and evaluated at a reduced temperature $T_\mathrm{r} = 0.7$, and proposed an approximate expression, different from (1), to evaluate this parameter.

Chen *et al.* [6] showed that large deviations can occur when using equation (1) to compute ξ at off-normal boiling temperatures. These authors recommended to use the temperature and entropy data, if they are available, to directly calculate ξ at the required temperature. Since 320 K is the approximate design temperature for condensation in an ORC, these authors calculated ξ at this temperature for fluids with $T_\mathrm{c} > 320$ K, and at 290 K by assuming that for $T_\mathrm{c} < 320$ K the condensation is designed to be at 290 K. Hærvig *et al.* [7] evaluated ξ at the temperature for which $\mathrm{d}^2 s^\mathrm{g}/\mathrm{d}T^2 = 0$ for dry fluids and at 293 K for wet fluids corresponding to approximately the condensing temperature. If the temperature at which $\mathrm{d}^2 s^\mathrm{g}/\mathrm{d}T^2 = 0$ does not occur between 293 K and T_c, then ξ was calculated at 293 K for dry fluids as well.

This work presents a thermodynamic study of the liquid-vapor saturation curve in a $T_\mathrm{r} - s^*$ diagram, where T_r is the reduced temperature and $s^* = s/R$, being R the gas constant. Our aim is to compare this saturation curve for different fluids in the scheme of the corresponding states principle (CSP) in order to analyze the possibility of characterizing the shape of the curve in terms of a reduced number of well-known parameters of the fluid. In this context, we note that the use of the dimensionless molar entropy s^* instead of s allows for obtaining dimensionless results in a CSP scheme without any loss of generality. The analysis is made from temperature and entropy liquid-vapor saturation data of the 121 fluids considered by the National Institute of Standards and Technology (NIST) program RefProp 9.1 [8].

The main objectives of this paper are: (i) Analyze the wet or dry character of working fluids in ORC cycles according to a CSP scheme. (ii) Identify the key parameters that determine the shape of the liquid-vapor saturation curve in a temperature-entropy representation. (iii) Analyze the different relations that arise between these parameters and other characteristic parameters of the fluids.

This work is structured as follows. In Section 2 we analyze the main features of the liquid-vapor saturation curve in a $T_{\rm r} - s^*$ diagram and introduce the relevant parameters in the problem like the reduced temperature $T_{\rm Mr}$ where the inverse of the slope of the vapor saturated branch of the $T_{\rm r} - s^*$ diagram reaches a maximum value $\xi^*_{\rm M}$. In Section 3 we present and discuss the results for the fluids considered in our study. We conclude with a brief Summary.

2. Theory

The liquid-vapor saturation curve in a $T_{\rm r} - s^*$ diagram presents a more or less inclined forward bell or dome shape with two branches, for all fluids considered in the RefProp 9.1 program [8]. The liquid saturated branch always presents a positive slope while there are two possibilities for the slope of the vapor saturated branch: either it is negative for any temperature between the triple and the critical point or it can present a zone with positive values. Furthermore, in all studied fluids, the inverse of the slope of the vapor saturated branch attains a maximum value $\xi^*_{\rm M} \equiv ({\rm d}s^{*\rm g}/{\rm d}T_{\rm r})_{T_{\rm Mr}}$ at a point M with reduced temperature $T_{\rm Mr} \approx 0.81$. The physical meaning of the maximum M becomes clear by noticing that those fluids with $\xi^*_{\rm M} < 0$ always have a negative slope for the vapor saturated branch and, consequently, they are wet fluids. Obviously, those fluids with $\xi^*_{\rm M} > 0$ present a zone around the maximum M with positive slope for the vapor saturated branch, behaving as dry fluids.

The significance of the point M in a $T_{\rm r} - s^*$ diagram is that at M this curve changes from concave to convex, i.e., $({\rm d}^2 s^{*\rm g}/{\rm d}T_{\rm r}^2)_{T_{\rm Mr}} = 0$. This suggests to take this inflection point as a reference in order to characterize the shape of the liquid-vapor saturation curve in a $T_{\rm r} - s^*$ diagram. In particular, one can take the dimensionless vaporization entropy $\Delta_{\rm v} s^*_{\rm M} = s^{*\rm g}_{\rm M} - s^{*\rm l}_{\rm M}$ as a measure of the 'width' of the curve, and the inverse of the slope $\xi^*_{\rm M} = ({\rm d}s^{*\rm g}/{\rm d}T_{\rm r})_{T_{\rm Mr}}$ as a measure of the 'inclination' of the curve. As mentioned above, we call 'wet' fluids those for which $\xi^*_{\rm M} < 0$ and 'dry' fluids those for which $\xi^*_{\rm M} > 0$. Obviously, fluids are either wet or dry but those with $|\xi^*_{\rm M}|$ close to zero can be

termed as isentropic. In the case of dry fluids there are two points at reduced temperatures T_{1r} and T_{2r}, ($T_{1r} < T_{Mr} < T_{2r}$), at which $\xi_1^* = \xi_2^* = 0$, being $\xi^*(T_r)$ positive for any value of T_r in the range (T_{1r}, T_{2r}), and negative out of this range. In the next Section we analyze T_{Mr}, T_{1r}, T_{2r}, ξ_M^* and $\Delta_v s_M^*$ in terms of the acentric factor, ω, and the critical parameters, (T_c, p_c, v_c), being p_c the critical pressure and v_c the critical molar volume, of the considered fluids. Besides its intrinsic thermodynamic interest, this analysis provides a set of semi-empirical guidelines which can help in the election of the working fluid in an ORC for a given operation design.

3. Results and Discussion

3.1. Wet and dry fluids

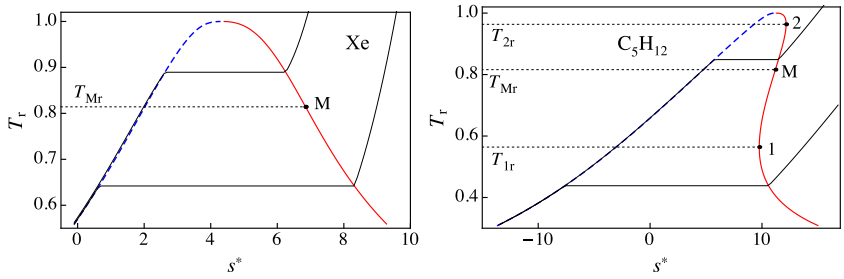

Figure 1: The liquid-vapor saturation curve in a $T_r - s^*$ diagram for xenon and pentane. The dashed blue lines correspond to the liquid saturated branch while the solid red lines correspond to the vapor saturated branch. The thin black lines correspond to different isobars, plotted here for illustrative reasons. All data have been obtained from RefProp 9.1 results [8].

Figure 1 shows the liquid-vapor saturation curve in a $T_r - s^*$ diagram for xenon and pentane. These curves are plotted from temperature and entropy data provided by the NIST RefProp 9.1 program [8]. Any fluid of the NIST program has a liquid-vapor saturation curve similar to one of these. For all fluids the liquid saturated branch present a positive slope for any temperature from the reduced triple point temperature, $T_{tp,r}$, to the critical one, $T_r = 1$. However, the vapor saturated branch presents two possibilities: either the slope

remains negative along the curve from $T_{\mathrm{tp,r}}$ to $T_{\mathrm{r}} = 1$ (xenon) or it can become positive in a given temperature range between $T_{\mathrm{tp,r}}$ and $T_{\mathrm{r}} = 1$ (pentane). 'Wet' fluids are those of the first type and 'dry' fluids are those of the second type. We note that these names are here used only in order to classify the fluids. Wet fluids always present condensation after the isentropic expansion in the turbine stage of a normal Rankine cycle while dry fluids may or may not present condensation depending on the condenser temperature. In Figure 1, two isobars are plotted for each fluid, in order to show their behavior in a $T_{\mathrm{r}} - s^*$ diagram.

The inverse of the slopes of the liquid and vapor saturated curves in a $T_{\mathrm{r}} - s^*$ diagram are given by

$$\frac{\mathrm{d}s^{*\mathrm{l}}}{\mathrm{d}T_{\mathrm{r}}} = \frac{c^{*\mathrm{l}}_{\mathrm{sat}}}{T_{\mathrm{r}}}\,, \tag{2}$$

$$\frac{\mathrm{d}s^{*\mathrm{g}}}{\mathrm{d}T_{\mathrm{r}}} = \frac{c^{*\mathrm{g}}_{\mathrm{sat}}}{T_{\mathrm{r}}}\,, \tag{3}$$

where $c^*_{\mathrm{sat}} = c_{\mathrm{sat}}/R$, c_{sat} being the molar heat capacity along the saturation line and, equations (2) and (3) are the dimensionless versions of the well known definitions of $c^{\mathrm{l}}_{\mathrm{sat}}$ and $c^{\mathrm{g}}_{\mathrm{sat}}$, respectively.

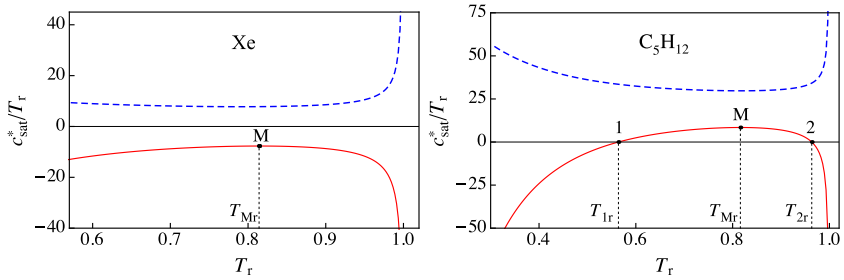

Figure 2: The slopes of the liquid-vapor saturation curve in a $T_{\mathrm{r}} - s^*$ diagram $c^*_{\mathrm{sat}}/T_{\mathrm{r}}$ vs. T_{r} for xenon and pentane. The dashed blue lines correspond to the liquid saturated branch while the solid red lines correspond to the vapor saturated branch. All data have been obtained from RefProp 9.1 results [8].

Figure 2 shows the slopes of the liquid-vapor saturation curve in a $T_{\mathrm{r}} - s^*$ diagram for xenon and pentane. One can see that $c^{*\mathrm{l}}_{\mathrm{sat}}/T_{\mathrm{r}}$ is always positive, but $c^{*\mathrm{g}}_{\mathrm{sat}}/T_{\mathrm{r}}$ is negative for xenon while it presents positive values for pentane. An

important remark is that, for all considered fluids, c^{*g}_{sat}/T_r presents a maximum at a point M, i.e.,

$$\left[\frac{d}{dT_r}\left(\frac{c^{*g}_{sat}}{T_r}\right)\right]_{T_{Mr}} = \left(\frac{d^2 s^{*g}}{dT_r^2}\right)_{T_{Mr}} = 0\,, \tag{4}$$

corresponding to an inflection point of the vapor saturated curve in the $T_r - s^*$ diagram. By defining

$$\xi^*_M = \left(\frac{ds^{*g}}{dT_r}\right)_{T_{Mr}} = \frac{c^{*g}_{M,sat}}{T_{Mr}}\,, \tag{5}$$

we find ($T_{Mr} = 0.8142, \xi^*_M = -7.6918$) for xenon and ($T_{Mr} = 0.8160, \xi^*_M = 8.4366$) for pentane. Therefore the sign of ξ^*_M gives directly the possibility that ds^{*g}/dT_r can change its sign between the triple and critical points. If $\xi^*_M < 0$ one has $\xi^* < 0$ at any temperature, while one has that $\xi^* > 0$ in a range of reduced temperatures around T_{Mr} if $\xi^*_M > 0$. In other words, ξ^*_M is a parameter characterizing the inclination forward of the liquid-vapor saturation curve in a $T_r - s^*$ diagram. Hence 'wet' fluids are those for which $\xi^*_M < 0$, and 'dry' fluids are those for which $\xi^*_M > 0$. In the latter case, as it is shown in Figure 1 for pentane, there are two points 1 and 2, at temperatures T_{1r} and T_{2r} (with $T_{1r} < T_{Mr} < T_{2r}$) for which $\xi^*_1 = \xi^*_2 = 0$. Consequently, only for reduced temperatures in the range (T_{1r}, T_{2r}) one has that $\xi^* > 0$. Rayegan and Tao [9] pointed out the importance of point 2 to determine the higher limit for the temperature and pressure of the evaporator in organic Rankine cycles

Table 1: Critical temperature T_c, acentric factor ω, critical molar volume v_c, slope of the liquid-vapor saturation curve at point M ξ^*_M, reduced temperature at point M T_{Mr}, reduced temperature at point 1 T_{1r}, reduced temperature at point 2 T_{2r}, and the entropy of vaporization at T_{Mr}, $\Delta_v s^*_M$. The data have been obtained from RefProp 9.1 [8]. The fluids are listed in increasing value of ξ^*_M.

Fluid	T_c[K]	ω	v_c[m^{3}kmol^{-1}]	ξ^*_M	T_{Mr}	T_{1r}	T_{2r}	$\Delta_v s^*_M$
methanol	513.38	0.5625	0.1138	−10.6364	0.7874	-	-	8.8708
heavy water	643.85	0.364	0.0563	−9.8770	0.8071	-	-	7.2551
water	647.1	0.3443	0.0559	−9.8460	0.8018	-	-	7.2546
ammonia	405.4	0.256	0.0757	−8.6109	0.8162	-	-	6.2501
hydrogen chloride	324.55	0.1288	0.0887	−8.3196	0.8228	-	-	5.2330
R41	317.28	0.2004	0.1075	−7.9926	0.8146	-	-	5.8814

Continued on next page

Table 1 – continued from previous page

Fluid	T_c[K]	ω	v_c[m^{3}kmol^{-1}]	ξ^*_M	T_{Mr}	T_{1r}	T_{2r}	$\Delta_v s^*_M$
carbon dioxide	304.13	0.2239	0.0941	−7.9381	0.8219	-	-	6.1289
R32	351.26	0.2769	0.1227	−7.7684	0.8198	-	-	6.3119
xenon	289.73	0.0036	0.119	−7.6918	0.8142	-	-	4.8280
krypton	209.48	−0.0009	0.0922	−7.6578	0.8124	-	-	4.8139
argon	150.69	−0.0022	0.0746	−7.6561	0.8117	-	-	4.8393
neon	44.49	−0.0387	0.0419	−7.3103	0.8012	-	-	4.7386
sulfur dioxide	430.64	0.2557	0.122	−7.2518	0.8202	-	-	6.2982
nitrous oxide	309.52	0.162	0.0974	−7.0185	0.8224	-	-	5.6947
R23	299.29	0.263	0.133	−6.8638	0.8205	-	-	6.2961
carbon monoxide	132.86	0.0497	0.0922	−6.8622	0.8091	-	-	5.2496
fluorine	144.41	0.0449	0.0641	−6.8234	0.8118	-	-	5.1817
nitrogen	126.19	0.0372	0.0894	−6.8113	0.8060	-	-	5.2014
hydrogen sulfide	373.1	0.1005	0.0981	−6.8028	0.8072	-	-	5.5701
oxygen	154.58	0.0222	0.0734	−6.7200	0.8054	-	-	5.1029
ethylene	282.35	0.0866	0.1309	−6.1541	0.8156	-	-	5.3553
deuterium	38.34	−0.136	0.058	−6.0597	0.7992	-	-	4.0694
R40	416.3	0.243	0.139	−6.0057	0.8311	-	-	5.3535
methane	190.56	0.0114	0.0986	−5.9212	0.7978	-	-	5.1420
nitrogen trifluoride	234	0.126	0.1263	−5.8855	0.8261	-	-	5.4018
R14	227.51	0.1785	0.1407	−5.7507	0.8153	-	-	6.0436
orthohydrogen	33.22	−0.218	0.0647	−5.5374	0.7814	-	-	3.7043
carbonyl sulfide	378.77	0.0978	0.135	−5.4797	0.8131	-	-	5.4778
ethanol	514.71	0.646	0.1686	−5.4382	0.8407	-	-	8.4402
parahydrogen	32.94	−0.219	0.0644	−5.4225	0.7856	-	-	3.6714
hydrogen	33.15	−0.219	0.0645	−5.3996	0.7873	-	-	3.6534
ethane	305.32	0.0995	0.1458	−4.8380	0.8145	-	-	5.4624
R22	369.3	0.2208	0.1651	−4.8229	0.8190	-	-	6.1328
R161	375.25	0.216	0.1592	−4.4255	0.8205	-	-	6.0484
propyne	402.38	0.204	0.1636	−3.5995	0.7971	-	-	6.4700
helium	5.2	−0.385	0.0575	−3.5483	0.7489	-	-	2.7423
R152a	386.41	0.2752	0.1795	−3.4813	0.8223	-	-	6.3362
R13	302	0.1723	0.1792	−3.3923	0.8226	-	-	5.8009
cyclopropane	398.3	0.1305	0.1628	−2.9929	0.8469	-	-	5.0172
R21	451.48	0.2061	0.1957	−2.9492	0.8180	-	-	6.0472
propylene	364.21	0.146	0.1833	−2.7352	0.8214	-	-	5.6326
R143a	345.86	0.2615	0.195	−2.4733	0.8183	-	-	6.3392
DME	400.38	0.196	0.1684	−2.4475	0.8198	-	-	5.9087
trifluoroiodomethane	396.44	0.176	0.2257	−2.4241	0.7992	-	-	6.2585
R134a	374.21	0.3268	0.1993	−1.5632	0.8172	-	-	6.8416
R12	385.12	0.1795	0.214	−1.5080	0.8043	-	-	6.1977
propane	369.89	0.1521	0.2	−1.3906	0.8214	-	-	5.6803
R125	339.17	0.3052	0.2092	−0.5398	0.8089	-	-	6.9552
acetone	508.1	0.3071	0.2128	−0.3538	0.8173	-	-	6.4984
RE143a	377.92	0.289	0.2151	−0.1089	0.8180	-	-	6.5302
sulfur hexafluoride	318.72	0.21	0.1968	−0.0175	0.8201	-	-	6.1658
R142b	410.26	0.2321	0.2253	0.1386	0.8155	0.7826	0.8462	6.2871
R11	471.11	0.1888	0.248	0.2340	0.7864	0.7395	0.8319	6.6258
R116	293.03	0.2566	0.225	0.4458	0.8128	0.7540	0.8650	6.5768
cis-butene	435.75	0.202	0.2356	0.9697	0.8248	0.7363	0.8955	5.8932
R1234ze	382.51	0.313	0.2331	1.0989	0.8034	0.7094	0.8829	7.1286
1-butene	419.29	0.192	0.2358	1.3717	0.8230	0.7149	0.9058	5.8589
R1234yf	367.85	0.276	0.2398	1.3815	0.8076	0.7062	0.8948	6.7509

Continued on next page

Table 1 – continued from previous page

Fluid	T_c[K]	ω	v_c[m^{3}kmol^{-1}]	ξ^*_M	T_{Mr}	T_{1r}	T_{2r}	$\Delta_v s^*_M$
R124	395.42	0.2881	0.2437	1.5614	0.8091	0.6960	0.9005	6.8123
trans-butene	428.61	0.21	0.2374	1.6935	0.8185	0.6976	0.9095	6.0656
isobutene	418.09	0.193	0.2398	1.8248	0.8193	0.6947	0.9131	5.9338
R141b	477.5	0.2195	0.255	2.3839	0.8112	0.6679	0.9199	6.3514
R115	353.1	0.248	0.2513	2.9004	0.8079	0.6487	0.9236	6.6389
isobutane	407.81	0.184	0.2577	3.0440	0.8223	0.6593	0.9341	5.8716
R1233zd	438.75	0.305	0.2725	3.0552	0.7975	0.6428	0.9195	7.1933
R123	456.83	0.2819	0.2781	3.4213	0.7994	0.6351	0.9276	6.9908
butane	425.12	0.201	0.2549	3.5432	0.8181	0.6409	0.9371	6.0497
R1216	358.9	0.333	0.2571	3.6838	0.8095	0.6459	0.9295	7.1882
R245fa	427.16	0.3776	0.2597	4.1683	0.8193	0.6489	0.9368	7.1450
R236fa	398.07	0.377	0.2758	4.6989	0.7995	0.6216	0.9347	7.6474
R114	418.83	0.2523	0.2947	5.4626	0.7781	0.6061	0.9414	7.3331
cyclopentane	511.72	0.201	0.2618	5.5240	0.8268	0.6345	0.9441	5.8153
R236ea	412.44	0.369	0.2691	5.7807	0.7922	0.5993	0.9439	7.7909
R245ca	447.57	0.355	0.2551	5.9462	0.8074	0.6127	0.9415	7.3125
R227ea	374.9	0.357	0.2861	6.0234	0.8071	0.6025	0.9488	7.3696
benzene	562.02	0.211	0.2563	6.1558	0.8252	0.6178	0.9543	5.9632
RE245cb2	406.81	0.354	0.3004	7.0324	0.7960	-	0.9513	7.5684
DEE	466.7	0.281	0.2808	7.0390	0.8045	0.5720	0.9547	6.8401
R218	345.02	0.3172	0.2994	7.2705	0.8054	0.5803	0.9526	7.1201
DMC	557	0.346	0.25	7.3867	0.8129	0.5890	0.9525	7.2388
R113	487.21	0.2525	0.3346	7.4017	0.7761	0.5499	0.9551	7.3494
RE245fa2	444.88	0.387	0.2913	7.9754	0.7977	0.5722	0.9508	7.7811
neopentane	433.74	0.1961	0.3058	8.1324	0.8216	-	0.9661	5.9799
isopentane	460.35	0.2274	0.3057	8.3612	0.8179	0.5693	0.9650	6.2384
pentane	469.7	0.251	0.311	8.4366	0.8160	0.5641	0.9635	6.4324
RC318	388.38	0.3553	0.3226	9.8443	0.7961	-	0.9626	7.7095
R365mfc	460	0.377	0.3125	10.1649	0.8151	0.5425	0.9643	7.2573
toluene	591.75	0.2657	0.3156	10.8934	0.8121	0.5540	0.9681	6.5371
cyclohexane	553.6	0.2096	0.3102	12.5657	0.8378	0.5530	0.9781	5.7219
hexane	507.82	0.299	0.3696	13.6814	0.8127	0.5152	0.9737	6.8090
isohexane	497.7	0.2797	0.3683	13.7711	0.8125	0.5202	0.9748	6.6775
RE347mcc	437.7	0.403	0.3817	14.2038	0.7903	-	0.9739	8.0751
perfluorobutane	386.33	0.371	0.3968	14.8856	0.7876	0.5095	0.9747	7.9636
m-xylene	616.89	0.326	0.3752	16.0966	0.8077	0.5123	0.9784	7.1226
p-xylene	616.17	0.324	0.3712	16.0973	0.8127	0.5109	0.9753	6.9021
ethylbenzene	617.12	0.305	0.3648	16.9260	0.8164	0.5066	0.9782	6.7379
o-xylene	630.26	0.312	0.3725	17.4037	0.8105	0.4969	0.9775	6.8488
methylcyclohexane	572.2	0.234	0.3676	18.5937	0.8222	0.4952	0.9823	6.1880
heptane	540.13	0.349	0.4319	19.2387	0.8059	0.4831	0.9818	7.2950
perfluoropentane	420.56	0.423	0.4726	22.8082	0.7793	0.4736	0.9852	8.8186
octane	569.32	0.395	0.4863	25.1117	0.8011	0.4580	0.9840	7.7575
isooctane	544	0.303	0.4717	25.2627	0.8145	0.4501	0.9886	6.7868
novec649	441.81	0.471	0.5208	28.6415	0.7003	-	0.9854	11.2642
MM	518.7	0.418	0.5334	28.6999	0.7645	-	0.9972	8.8837
nonane	594.55	0.4433	0.5525	31.1834	0.7963	0.4378	0.9865	8.2254
propylcyclohhexane	630.8	0.326	0.4854	31.4514	0.8077	0.4338	0.9902	7.0561
decane	617.7	0.4884	0.6098	37.1920	0.7864	0.4207	0.9880	8.7914
undecane	638.8	0.539	0.6601	43.7309	0.7863	0.4074	0.9906	9.0895
MDM	564.09	0.529	0.9213	48.9411	0.7539	0.3667	0.9936	10.2178
dodecane	658.1	0.574	0.7519	50.0562	0.7743	-	0.9939	9.7719

Continued on next page

Table 1 – continued from previous page

Fluid	T_c[K]	ω	v_c[m^{3}kmol^{-1}]	ξ^*_M	T_{Mr}	T_{1r}	T_{2r}	$\Delta_v s^*_M$
D4	586.49	0.592	0.9661	52.9243	0.7727	-	0.9936	10.1578
MD2M	599.4	0.668	1.0933	66.2116	0.7353	-	0.9938	11.7829
D5	619.23	0.658	1.2673	73.8466	0.7473	-	0.9939	11.4233
methyl palmitate	755	0.91	1.1148	86.6279	0.7388	-	0.9924	13.4264
methyl linolenate	772	1.14	1.1802	87.0511	0.7625	0.3649	0.9918	14.3799
MD3M	628.36	0.722	1.4582	92.3726	0.7165	-	0.9940	13.2612
methyl linoleate	799	0.805	1.237	96.4907	0.7361	0.3468	0.9942	12.9567
methyl oleate	782	0.906	1.2303	97.9157	0.7395	0.3480	0.9936	13.4667
methyl stearate	775	1.02	1.259	100.2849	0.7366	-	0.9929	14.3641
D6	645.78	0.736	1.5941	104.5704	0.6897	-	0.9947	14.2989
MD4M	653.2	0.825	1.6067	106.7797	0.7384	-	0.9967	13.1683

Figure 3 shows plots of ξ^*_M vs. the acentric factor, ω ($\omega = -1.0 - \log_{10} p_r$ at $T_r = 0.7$), and the critical parameters T_c, p_c, and v_c for the 121 fluids included in the RefProp 9.1 program [8] and listed in table 1. Figure 3(a) shows a plot of ξ^*_M vs. ω. Although there is no correlation between ξ^*_M and ω, one can observe that there are no dry fluids with acentric factor below $\omega \approx 0.180$ [isobutane is the dry fluid ($\xi^*_M = 3.0440$) with the smallest acentric factor ($\omega = 0.184$)], while one can find wet fluids below and above this value. Figure 3(b) shows a plot of ξ^*_M vs. T_c. One can see that there is no correlation between ξ^*_M and T_c. However, there are practically no dry fluids with a critical temperature below 340 K [R116 is the only dry fluid ($\xi^*_M = 0.4458$) with T_c (293.03 K) below 340 K] while one can find wet fluids below and above this value. Figure 3(c) shows a plot of ξ^*_M vs. p_c. One can observe that there is no correlation between ξ^*_M and p_c. However, there are no dry fluids with a critical pressure above 4910 kPa [DMC is the dry fluid ($\xi^*_M = 7.3867$) with the largest p_c value ($p_c = 4908.8$ kPa)] while one can find wet fluids below and above this value. Although from Figures 3(a)-(c) no correlations can be identified neither for dry fluids nor for wet fluids, it becomes apparent that the behavior of ξ^*_M vs. ω, T_c, and p_c for dry fluids is clearly different from the one for wet fluids.

Finally, figure 3(d) shows a plot of ξ^*_M vs. v_c. This figure shows that there is a threshold value of the critical molar volume, $v_{c,0} \approx 0.22$ m^3 kmol^{-1}, separating wet and dry fluids: wet fluids for $v_c < v_{c,0}$ and dry fluids for $v_c > v_{c,0}$, with the only exception of CF_3I (trifluoroiodomethane), a wet fluid ($\xi^*_M = -2.4241$)

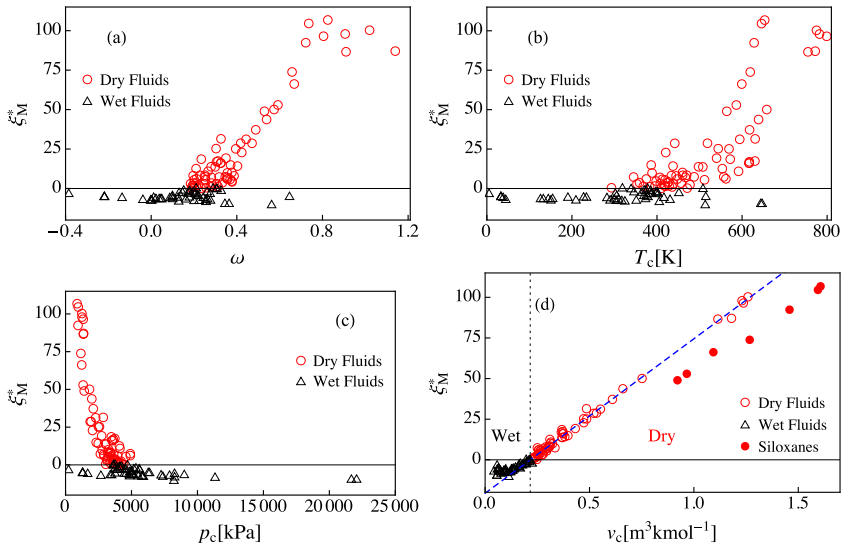

Figure 3: Plot of ξ^*_M vs. (a) the acentric factor ω, (b) the critical temperature T_c, (c) the critical pressure p_c, and (d) the critical molar volume v_c. Black empty triangles correspond to wet fluids ($\xi^*_M < 0$) while red empty circles correspond to dry fluids ($\xi^*_M > 0$). The red filled circles in (d) correspond to the oddball dry fluids (see text). All data have been obtained from RefProp 9.1 results [8]. The dashed line in (d) is obtained from equation (6). The vertical dotted line in (d) indicates the critical molar volume $v_{c,0} = 0.2164$ m^3 kmol^{-1} that separates wet fluids from dry fluids.

with $v_c = 0.2257$ m^3 kmol^{-1}. There is no clear correlation between ξ^*_M and v_c for wet fluids, while ξ^*_M seems to increase linearly with v_c for dry fluids. By excluding seven oddball dry fluids (all of them siloxanes with large v_c values: D4, D5, D6, MDM, MD2M, MD3M, and MD4M), the following linear fit can be obtained for dry fluids:

$$\xi^*_M = 20.57 \left(\frac{v_c}{v_{c,0}} - 1 \right) , \tag{6}$$

with $v_{c,0} = 0.2164$ m^3 kmol^{-1} and a coefficient of determination R^2 of 0.995. Equation (6) is plotted in figure 3(d) with a dashed line. This equation suggests the introduction of the dimensionless parameter

$$d = \frac{v_c}{v_{c,0}} - 1 , \tag{7}$$

in order to predict the wet or dry character of a fluid only through the knowledge of its critical molar volume: $d < 0$ for wet fluids and $d > 0$ for dry fluids.

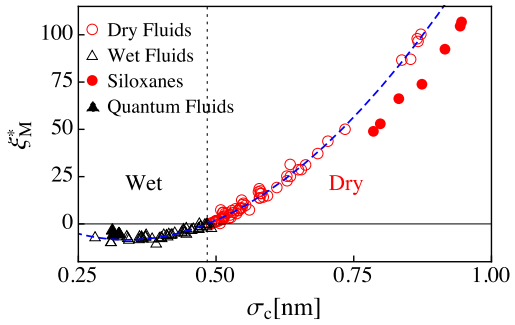

Figure 4: Plot of ξ^*_M vs. the intermolecular separation at zero potential energy σ_c. The symbols are RefProp 9.1 results [8] and the dashed line represents equation (8). Black triangles correspond to wet fluids while red circles correspond to dry fluids. Filled symbols correspond to the oddball dry fluids (circles) and the quantum fluids (triangles) (see text). The vertical dotted line indicates the value $\sigma_{c,0} = 0.484$ nm.

Smit [10] has shown that the critical molar volume v_c of a Lennard-Jones fluid is related to the intermolecular separation at zero potential energy σ_c via $N_A\sigma_c^3/v_c = 0.317$, where N_A is the Avogadro number. This fact suggests that ξ^*_M should be correlated with σ_c. Figure 4 represents ξ^*_M vs. σ_c. This figure shows that there is a fair nonlinear correlation between ξ^*_M and σ_c. In particular, by excluding the seven oddballs dry fluids of figure 3(d) (siloxanes with large v_c values: D4, D5, D6, MDM, MD2M, MD3M, and MD4M) and the five quantum fluids (hydrogen, orthohydrogen, parahydrogen, deuterium and helium), the following cubic fit can be obtained for the remaining 109 fluids (both dry and wet):

$$\xi^*_M = 40.4747 - 295.354(\sigma_c/\text{nm}) + 465.566(\sigma_c/\text{nm})^2 - 57.8077(\sigma_c/\text{nm})^3\,, \quad (8)$$

with a coefficient of determination R^2 of 0.995. Equation (8) is plotted in figure 4 by a dashed line. From equation (8) one obtains that $\xi^*_M = 0$ for $\sigma_{c,0} = 0.484$ nm, which corresponds to a critical molar volume $v_{c,0} = 0.216$ m^3 kmol^{-1}, in agreement with the above reported value for $v_{c,0}$. This analysis seems to

indicate that the wet or dry character of a fluid is mainly correlated with its molecular size (measured by σ_c) instead of its molecular complexity (measured by ω). The 'five quantum fluids' excluded from the fit presented in equation (8) are wet fluids with very low molecular weight that, due to quantum effects, can show a behavior that may differ from that of the rest of the fluids. In figure 4 the differences between the quantum fluids and the remaining wet fluids are small although noticeable. Of course, the differences between the oddball dry fluids (siloxanes with large v_c) and the other dry fluids are much larger as one can observe in figure 4. From this figure one can infer that the ξ_M^* results for the siloxanes are also correlated with σ_c but with a different correlation, probably due to effects that are specific to the siloxanes family of fluids. The analysis of these effects lies out of the scope of the present work.

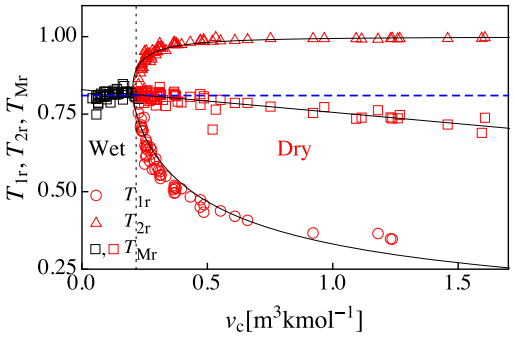

Figure 5: Plot of the reduced temperatures T_{Mr} (squares), T_{1r} (circles), and T_{2r} (triangles) vs. the critical molar volume v_c. Black squares correspond to wet fluids ($\xi_M^* < 0$, $v_c < v_{c,0}$) and red symbols correspond to dry fluids ($\xi_M^* > 0$, $v_c > v_{c,0}$). The horizontal dashed line indicates the reduced temperature $T_r = 0.81$. The vertical dotted line indicates the critical molar volume $v_{c,0} = 0.2164$ m^3 kmol^{-1} that separates wet fluids from dry fluids.The thin solid lines correspond to the fits (9) and (10) (see text). All data have been obtained from RefProp 9.1 results [8].

Figure 5 shows a plot of T_{1r}, T_{2r}, and T_{Mr} vs. v_c. As one can observe, there is a fair correlation between these reduced temperatures and the critical molar volume. In particular, one has that for most wet and dry fluids T_{Mr} lie into the reduced temperature range 0.79 – 0.83 with a mean value of $T_{Mr} \approx 0.81$. As

a general rule for dry fluids, $T_{1\mathrm{r}}$ decreases and $T_{2\mathrm{r}}$ increases as v_{c} increases, in accordance with the fact that ξ^*_{M} becomes more positive as v_{c} increases, i.e., the $\xi^* = c^{*\mathrm{g}}_{\mathrm{sat}}/T_{\mathrm{r}}$ curve is shifted towards larger positive values. In order to better illustrate the behavior observed in Figure 5 for dry fluids, we have obtained the following linear fit for T_{Mr}:

$$T_{\mathrm{Mr}} = 0.8288 - 0.01581\frac{v_{\mathrm{c}}}{v_{\mathrm{c},0}}\,, \tag{9}$$

with a coefficient of determination R^2 of 0.719. Furthermore, a fit of $v_{\mathrm{c}}/v_{\mathrm{c},0}$ in terms of $T_{2\mathrm{r}}$ yields

$$\frac{v_{\mathrm{c}}}{v_{\mathrm{c},0}} = -0.1456 + 0.5122 f(T_{2\mathrm{r}})\,, \tag{10}$$

with a coefficient of determination R^2 of 0.732, and where we have chosen

$$f(T_{\mathrm{r}}) = -\frac{\mathrm{d}}{\mathrm{d}T_{\mathrm{r}}}\left[\frac{(1-T_{\mathrm{r}})^{0.38}}{T_{\mathrm{r}}}\right] = \frac{(1-T_{\mathrm{r}})^{0.38}}{T_{\mathrm{r}}^2} + \frac{0.38}{T_{\mathrm{r}}(1-T_{\mathrm{r}})^{0.62}} \tag{11}$$

using an heuristic approach, motivated by equation (3) and the Watson relation [3, 4] applied to the temperature dependence of $\Delta_{\mathrm{v}}s^* = \Delta_{\mathrm{v}}h_{\mathrm{r}}/T_{\mathrm{r}}$ (see below). This choice of $f(T_{\mathrm{r}})$ as a fitting function in (10) yields fairly good results not only for $v_{\mathrm{c}}/v_{\mathrm{c},0}$ in terms of $T_{2\mathrm{r}}$ but also in terms of $T_{1\mathrm{r}}$ as one can see in Figure 5.

3.2. The entropy of vaporization at the inflection point of the vapor saturated curve in a $T_{\mathrm{r}} - s^*$ diagram

The 'width' of the liquid-vapor saturation curve in a $T_{\mathrm{r}} - s^*$ diagram at a reduced temperature T_{r} is given by the entropy of vaporization $\Delta_{\mathrm{v}}s^*(T_{\mathrm{r}}) = s^{*\mathrm{g}}(T_{\mathrm{r}}) - s^{*\mathrm{l}}(T_{\mathrm{r}})$. Then, we propose the entropy of vaporization at the reduced temperature T_{Mr},

$$\Delta_{\mathrm{v}}s^*_{\mathrm{M}} \equiv \Delta_{\mathrm{v}}s^*(T_{\mathrm{Mr}})\,, \tag{12}$$

as a parameter characterizing the 'mean width' of the liquid-vapor saturation curve in a $T_{\mathrm{r}} - s^*$ diagram. Figures 6(a) and 6(b) show plots of $\Delta_{\mathrm{v}}s^*_{\mathrm{M}}$ vs. the critical molar volume v_{c} and the acentric factor ω, respectively. In figure 6(a) one can observe that there is no correlation between $\Delta_{\mathrm{v}}s^*_{\mathrm{M}}$ and v_{c}. However,

figure 6(b) shows that there is a moderate correlation between $\Delta_{\rm v} s^*_{\rm M}$ and ω. In this context, Velasco *et al.* [11] have recently proposed the equation

$$\Delta_{\rm v} h_{\rm r} = \left(7.2729 + 10.4962\,\omega + 0.6061\,\omega^2\right)\left(1 - T_{\rm r}\right)^{0.38} . \qquad (13)$$

for providing the reduced enthalpy of vaporization, $\Delta_{\rm v} h_{\rm r} = \Delta_{\rm v} h / R T_{\rm c}$, in terms of the reduced temperature and the acentric factor. Taking into account that $\Delta_{\rm v} s^* = \Delta_{\rm v} h_{\rm r} / T_{\rm r}$, by using equation (13) and assuming $T_{\rm Mr} \approx 0.81$, one obtains,

$$\Delta_{\rm v} s^*_{\rm M} \approx \frac{\Delta_{\rm v} h_{\rm r}(0.81)}{0.81} = 4.77693 + 6.89403\,\omega + 0.398094\,\omega^2 . \qquad (14)$$

Equation (14) is plotted in figure 6(b) with a dashed line, showing a fair agreement with the RefProp 9.1 results for $\Delta_{\rm v} s^*_{\rm M}(\omega)$. Clearly, the deviations between the $\Delta_{\rm v} s^*_{\rm M}$ data and the results of equation (14) represented in figure 6(b) are mainly due to deviations of $T_{\rm Mr}$ with respect to the value $T_{\rm Mr} \approx 0.81$ considered in equation (14).

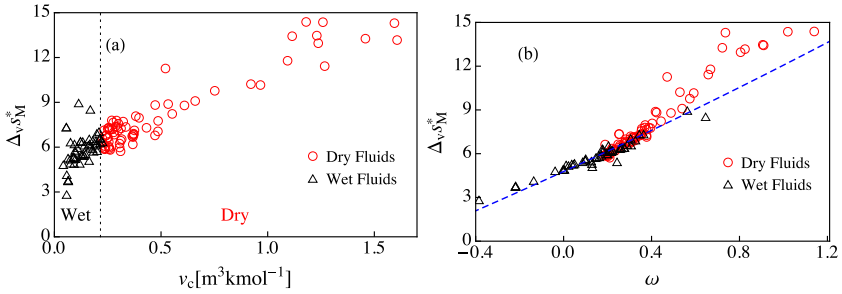

Figure 6: Plot of $\Delta_{\rm v} s^*_{\rm M}$ vs. (a) the critical molar volume $v_{\rm c}$ and (b) the acentric factor ω. Black triangles correspond to wet fluids while red circles correspond to dry fluids. The dashed line corresponds to equation (14) (see text). The symbols are RefProp 9.1 results [8]. The vertical dotted line in (a) indicates the critical molar volume $v_{\rm c,0} = 0.2164$ m^3 kmol^{-1} that separates wet fluids from dry fluids.

4. Summary

To summarize, the occurrence of an inflection point M, at a reduced temperature $T_{\rm Mr}$, in the saturated vapor curve $s^{*\rm g} = s^{*\rm g}(T_{\rm r})$ allows one to characterize

the shape of the liquid-vapor saturation curve in the $T_\mathrm{r} - s^*$ diagram. More concretely, the slope at this point, $\xi^*_\mathrm{M} = (\mathrm{d}s^{*\mathrm{g}}/\mathrm{d}T_\mathrm{r})_{T_\mathrm{Mr}}$, provides information about the 'inclination forward' of the liquid-vapor saturation curve while the entropy of vaporization at this point, $\Delta_\mathrm{v} s^*_\mathrm{M} = s^{*\mathrm{g}}(T_\mathrm{Mr}) - s^{*\mathrm{l}}(T_\mathrm{Mr})$, gives information about its 'width'. Furthermore, the fact that the parameter ξ^*_M becomes negative for some fluids and positive for others, allows one to classify the fluids like wet or dry, respectively. For those fluids for which $\xi^*_\mathrm{M} > 0$ (dry fluids), there are two temperatures T_1r and T_2r, with $T_\mathrm{1r} < T_\mathrm{Mr} < T_\mathrm{2r}$, at which $\xi^* = 0$ and, therefore, $\xi^* > 0$ at any reduced temperature in the range $(T_\mathrm{1r}, T_\mathrm{2r})$.

Using data for the 121 fluids considered in the RefProp 9.1 program we find that the sign of ξ^*_M is related to the molar critical volume, v_c, of the fluid. In particular, there is a threshold value, $v_{\mathrm{c},0} \approx 0.22$ m^3/kmol, below which the fluids are wet ($\xi^*_\mathrm{M} < 0$) and above which the fluids are dry ($\xi^*_\mathrm{M} > 0$). Furthermore, for dry fluids, ξ^*_M presents a linear correlation with v_c. Since v_c is related to the molecular diameter, one relevant conclusion of this work is that the wet ($\xi^*_\mathrm{M} < 0$) or dry ($\xi^*_\mathrm{M} > 0$) behavior of a fluid is related to its molecular size. We also find that the reduced temperatures T_Mr, T_1r and T_2r are correlated with v_c. For wet fluids ($v_\mathrm{c} < v_{\mathrm{c},0}$) the values of T_Mr are noisily distributed around $T_\mathrm{Mr} \approx 0.81$, while for dry fluids ($v_\mathrm{c} > v_{\mathrm{c},0}$) the values of T_Mr are also noisily distributed around $T_\mathrm{Mr} \approx 0.81$ between $v_{\mathrm{c},0}$ and $v_\mathrm{c} \approx 0.5$ m^3/kmol while they decrease slightly for higher v_c values. In addition, we also find that, for dry fluids, T_1r decreases and T_2r increases as v_c increases, according with the fact that ξ^*_M becomes more positive as v_c increases. In other words, the difference $T_\mathrm{2r} - T_\mathrm{1r}$ increases as v_c increases. Finally, we have shown that the entropy of vaporization $\Delta_\mathrm{v} s^*_\mathrm{M}$ is correlated with the acentric factor ω. Thus, the shape of the liquid-vapor saturation curve in a temperature-entropy diagram of a given fluid is mainly governed by its molar critical volume and its acentric factor.

Acknowledgements

We thank financial support by Junta de Castilla y León of Spain under Grant SA017P17.

References

[1] J. Bao, L. Zhao, A review of working fluid and expander selections for organic rankine cycle, Renewable and Sustainable Energy Reviews 24 (Supplement C) (2013) 325 – 342. doi:https://doi.org/10.1016/j.rser.2013.03.040.
URL http://www.sciencedirect.com/science/article/pii/S1364032113001998

[2] B.-T. Liu, K.-H. Chien, C.-C. Wang, Effect of working fluids on organic rankine cycle for waste heat recovery, Energy 29 (8) (2004) 1207 – 1217. doi:http://dx.doi.org/10.1016/j.energy.2004.01.004.
URL http://www.sciencedirect.com/science/article/pii/S0360544204000179

[3] K. Watson, Prediction of critical temperatures and heats of vaporization, Ind. Eng. Chem. 23 (4) (1931) 360–364.

[4] F. L. Román, J. A. White, S. Velasco, A. Mulero, On the universal behavior of some thermodynamic properties along the whole liquid-vapor coexistence curve, J. Chem. Phys. 123 (12) (2005) 124512–1–6. doi:10.1063/1.2035084.

[5] C. Invernizzi, P. Iora, P. Silva, Bottoming micro-rankine cycles for micro-gas turbines, Applied Thermal Engineering 27 (1) (2007) 100 – 110. doi:https://doi.org/10.1016/j.applthermaleng.2006.05.003.
URL http://www.sciencedirect.com/science/article/pii/S1359431106001724

[6] H. Chen, D. Y. Goswami, E. K. Stefanakos, A review of thermodynamic cycles and working fluids for the conversion of low-grade heat, Renewable and Sustainable Energy Reviews 14 (9) (2010) 3059–3067.

[7] J. Hærvig, K. Sørensen, T. Condra, Guidelines for optimal selection of working fluid for an organic rankine cycle in relation to waste heat recovery, Energy 96 (2016) 592 – 602. doi:http://dx.doi.org/10.1016/j.energy.2015.12.098.
URL http://www.sciencedirect.com/science/article/pii/S0360544215017430

[8] E. W. Lemmon, M. L. Huber, M. O. McLinden, NIST Standard Reference Database 23: Reference fluid thermodynamic and transport properties-REFPROP, version 9.1, National Institute of Standards and Technology, Standard Reference Data Program, Gaithersburg (2013).

[9] R. Rayegan, Y. Tao, A procedure to select working fluids for solar organic rankine cycles (orcs), Renewable Energy 36 (2) (2011) 659 – 670. doi:https://doi.org/10.1016/j.renene.2010.07.010.
URL http://www.sciencedirect.com/science/article/pii/S0960148110003344

[10] B. Smit, Phase diagrams of lennard-jones fluids, J. Chem. Phys. 96 (11) (1992) 8639–8640.

[11] S. Velasco, M. J. Santos, J. A. White, Extended corresponding states expressions for the changes in enthalpy, compressibility factor and constant-volume heat capacity at vaporization, The Journal of Chemical Thermodynamics 85 (0) (2015) 68 – 76. doi:http://dx.doi.org/10.1016/j.jct.2015.01.011.
URL http://www.sciencedirect.com/science/article/pii/S0021961415000208